Plastic Deformation of the γ Phase in Isotactic Polypropylene in Plane-Strain Compression

E. Lezak, Z. Bartczak,* and A. Galeski

Centre of Molecular and Macromolecular Studies, Polish Academy of Science, Sienkiewicza 112, 90−363 Lodz, Poland

Received March 16, 2006; Revised Manuscript Received May 5, 2006

ABSTRACT: Morphology and deformation behavior of samples of iPP homopolymer containing exclusively γ-modification with only minor traces of α-crystals, obtained by isothermal crystallization at high pressure of 200 MPa, were investigated. It was found that the growth of γ-lamellae is initiated on "seeds" consisting of a spine of single α-lamella and several shorter α-lamellae branching at the angle of 80°. Epitaxial growth of γ-lamellae on (010) faces of α-parent and daughter lamellae of the seed leads to the formation of immature spherulites, which eventually fill completely the sample volume. The plane-strain and uniaxial compression tests demonstrated higher modulus, higher yield stress and flow stress, yet slightly lower ultimate strain of γ-iPP as compared to α−iPP. During plastic deformation numerous fine shear bands, initiated by the interlamellar shear of the amorphous layers start to develop already at the yield point. Their propagation across the sample causes a limited destruction of γ-lamellae oriented perpendicularly to the direction of the band. Destroyed fragments of crystallites transform partially into a smectic phase. No $\gamma-\alpha$ phase transformation was detected. With increasing strain the shear bands multiply and tilt gradually toward the flow direction. Lamellae, already fragmented within shear bands, undergo kinking and rotation, resulting in the formation of a chevron-like lamellar morphology. Simultaneously, a relatively weak one-component crystalline texture is developed. This texture is described by the orientation of *c* crystallographic axis along the constrained direction, *b* axis 10−30° away from the loading direction toward the flow direction, and *a* axis 10−30° away from FD. Both crystalline texture and lamellae orientation are developed due to the activity of the same deformation mechanism—the interlamellar slip produced by the shear within interlamellar amorphous layers. Activity of any crystallographic deformation mechanism within crystalline component was not detected. The interlamellar amorphous shear appears the primary deformation mechanism of γ-iPP. The other identified mechanism, γ-smectic phase transformation, plays a minor, supplementary role in the deformation sequence.

1. Introduction

Isotactic polypropylene (iPP) is a polymorphic material which can crystallize in three crystalline forms: monoclinic α, hexagonal β, and orthorhombic γ. Moreover, under some conditions, e.g. under very high undercooling, a mesophase, usually called "smectic", can be formed instead of a crystalline phase. The most common crystal modification, obtained at typical processing conditions of iPP is the monoclinic α-form.[1] Many experimental observations suggest that α-modification is the most stable crystalline form of iPP.[2] The α-iPP reveals the lamellar branching of crystallographic origin which is an unique feature in polymer crystallography. Such branching leads to formation of two population of lamellae of radial and tangential orientation in the growing spherulite[3,4] and results in so-called "crosshatched" lamellar morphology.

Another crystalline modification of iPP, γ, though first recognized a few decades ago,[5] became studied more extensively much later. The γ-form is rarely observed in samples of iPP homopolymer crystallized at typical conditions under atmospheric pressure. The crystallization in the γ-form was, however, observed in samples of "defective" polymer: either material of very low molecular weight (1000−3000 g/mol),[6−8] or PP demonstrating relatively short isotactic sequences due to copolymerization with small amount of 1-olefine counits[9−15] or due to some stereo- and regioirregularities as those present in high molecular weight iPP prepared with metalocene catalyst.[16,17]

Samples with large content of γ-modification were obtained also by crystallization of highly stereoregular iPP homopolymers under high pressure.[5,18−26] At moderate pressures the crystallization of iPP in both α- and γ-forms was observed while at crystallization pressure reaching 200 MPa the γ-phase becomes predominant.[24] Higher pressure results in crystallization exclusively in the γ form.

The structure of γ-iPP crystal is very unusual in that the chain axes in the crystal are not aligned in one direction as in other known polymer crystals. Instead, the orthorhombic unit cell of the γ-modification is formed by bilayers, each composed of parallel helices.[19−21] The direction of the chain axis in adjacent bilayers is tilted by approximately 80° against each other and approximately 40° with respect to the crystallographic *b* axis, coinciding with lamella normal.[19−21] The angle between chains in adjacent bilayers is the same angle as that observed between mother and daughter lamella of the α-iPP.[27] Such a nonparallel chain arrangement is an unique packing arrangement for polymers, although it is known, e.g., for fatty acids.[28]

While the crystallographic structure of the γ-form has been already solved, still very little is known about mechanical properties of crystals of this modification or the mechanical performance of materials containing γ-modification as a major crystalline form. Turner-Jones et al.[29] suggested that upon application of the mechanical stress the γ-phase readily transforms to the α-phase; however, there are no other reports in the literature.

* Corresponding author. Telephone: +48 (42) 680-3237. E-mail: bartczak@bilbo.cbmm.lodz.pl.

10.1021/ma0605907 CCC: $33.50
Published on Web 06/09/2006

The goal of the presented study was to investigate the mechanical properties of iPP crystallized in γ-form and to find micromechanisms active during plastic deformation of γ-crystals. This problem seems to be very interesting due to the unique nonparallel chain arrangement, which probably constrains or even exclude some of mechanisms allowed in other polymer crystals, like, e.g., the crystallographic slip in the direction of chain, commonly very active in deformation of polymeric crystals.

Samples containing exclusively crystals of γ-form were prepared by crystallization of iPP homopolymer at high pressure. As a deformation mode, the plane-strain compression was chosen. This mode is kinematically similar to tension, leading to axial flow of the polymer in the direction perpendicular to a compressive load.[30] However, it has several advantages over other modes of deformation. The two most important are that (i) the deformation process is macroscopically homogeneous in the entire strain range, with no instabilities like necking usually observed in tension and (ii) deformation is virtually cavity-free, since the compressive stress component prevents noticeable cavitation, while existing accidental cavities are quickly healed by advancing compression. This is owing to the fact that the deformation process is not obscured by any unwanted side effects and can be studied effectively in a very wide range of strain. The true stress−true strain curves, characterizing the deformation process, can be obtained in this deformation mode relatively easily. Furthermore, it should be also mentioned that constraints imposed on a sample during its compression in the plane-strain experiment eliminate also most of the problems which could be encountered in uniaxial compression (which is also a cavity-free mode), as those related to sample barreling or radial cracking at high strains. Nevertheless, a few uniaxial compression tests was also performed for comparison of mechanical response in plane-strain and uniaxial conditions.

2. Experimental Section

2.1. Materials and Sample Preparation. The material used in this investigation was a commercial-grade isotactic polypropylene homopolymer, MalenP, F-401 (M_w = 297 200, M_n = 56 400, Melt flow index MFI (190 °C/2.16 kg) = 3 g/10 min, isotactic index > 95%), provided by Basell-Orlen Polyolefins (Poland). The polymer was stabilized properly against oxidation and thermal degradation.

Samples of γ−phase in the form of disks or rods of 9.5 mm in diameter and 3−20 mm high were prepared by crystallization of iPP at high pressure using a crystallization cell consisting of a barrel and two pistons, and a loading frame of the tensile testing machine (Instron 1114). Details of the high-pressure cell are given elsewhere.[31] The computer control of the loading frame allowed to maintain the constant hydrostatic pressure inside the cell with an accuracy of 0.2 MPa despite the volume shrinkage due to crystallization. The temperature of the sample in the cell was controlled with an accuracy of 0.1 °C.

The cell with the sample inside was pressurized first to approximately 400 MPa for few seconds in order to tighten copper seals. Then the pressure was reduced to and maintained at 200 MPa. The pressurized cell was heated to temperature of 248 °C in order to melt the iPP sample inside ($T_m°$ = 242.1 °C at p = 200 MPa[25]) and kept at this temperature for 3 min. Then the temperature was reduced to the desired crystallization temperature, set within the range 170−200 °C. Depending on the crystallization temperature the sample was allowed to crystallize at these conditions for 1−4 h to complete transformation. Next, the cell was cooled to the room temperature and then unloaded.

2.2. Compression Experiments. Plane-strain compression tests were performed using an universal tensile testing machine (Instron, model 5582) and a compression tool of the type of channel-die,[32,33] equipped with a strain gauge. This compression tool was a set of a lower die with a wide rectangular channel cut across the die and an upper plunger fitting the channel in the lower die. The size of the channel in the lower die was 6 mm in width (i.e., along the constrained direction, CD), 4 mm in length (along the flow direction, FD), and 6 mm in depth (along the loading direction, LD). This allowed samples up to 4 mm high to be compressed in plane strain-conditions. Details of the channel-die used is given in ref 33.

The specimens for compression experiments were prepared from high-pressure crystallized samples of γ-iPP by careful machining to the form of rectangular prism 6 × 4 × H mm (CD × FD × LD; where H = 2−4 mm). The surfaces contacting with the die and the plunger were lubricated to reduce friction forces during deformation.

Supplementary uniaxial compression tests were performed using the same testing machine equipped with flat compression platens. Disk-shaped samples of 9 mm in diameter and 4 mm high, properly lubricated, were used in these experiments.

Both plane-strain and uniaxial compression experiments were performed at a constant true strain rate of 0.05 min^{-1} at room temperature. For structural studies several specimens were compressed in the plane-strain mode to the preselected true strains of e = 0, 0.07, 0.18, 0.41, 0.71, and 0.93 (true strain e = ln λ; compression ratio up to λ = 2.6).

2.3. Characterization. DSC. Thermal analysis was carried out with a DSC apparatus (TA 2920, Thermal Analysis). The overall crystallinity was estimated on the basis of the heat of melting recorded during heating with a rate of 10 °C/min. The heat of melting of 100% crystalline α- and γ-iPP of $\Delta h_f(\alpha)$ = 209 J/g and $\Delta h_f(\gamma)$ = 190 J/g, respectively were assumed for calculations.[34,25]

WAXS. Computer-controlled X-ray diffractometer (DRON) equipped with a pole figure attachment, coupled to a sealed-tube source of filtered Cu K_α radiation, operating at 50 kV and 30 mA (Phillips) was used for X-ray measurements. The Θ−2Θ scans were collected with the step of 0.05°. From obtained diffractograms the phase composition, including content of the γ-phase was estimated. For accurate determination of phase structure the peak separation procedure was applied. The program OptiFit[35,36] based on multi-criteria optimization algorithm was used for this purpose.

The texture of deformed samples was studied using the X-ray pole figure technique (for overview of this technique see, e.g., ref 37). The specimens in the form of slices approximately 2 mm thick were cut out from the deformed samples in the plane perpendicular to the loading direction (LD). The (111), (008), and (117) crystal planes of the orthorhombic γ−form of iPP were analyzed (diffraction maxima centered around 2Θ = 13.84, 16.72, and 20.07°, respectively) and the respective pole figures were constructed. These pole figures were plotted with the POD program (Los Alamos National Lab, NM). Other details of the experimental procedure were described elsewhere.[38]

SAXS. Lamellar structure of raw, pressure crystallized as well as deformed samples was probed by 2-dimensional small-angle X-ray scattering (2-D SAXS). The 1.1 m long Kiessig-type camera was equipped with a tapered capillary collimator (X-ray Optical Systems) combined with additional pinholes (300 μm in diameter) forming the beam, and an imaging plate as a detector (Fuji). The camera was coupled to a X-ray source (sealed-tube, fine point Cu Kα, Ni-filtered radiation, operating at 50 kV and 40 mA; Philips). The time of collection of the pattern was usually around 3 h. Exposed imaging plates were read with Phosphor Imager SI scanner and ImageQuant software (Molecular Dynamics). Long periods (LP) in the direction of interest were determined from appropriate one-dimensional sections of 2-D patterns. LP was calculated using Bragg's law from the position of the maximum of background and Lorentz corrected curves.

SEM. The specimens for microscopic observations were prepared in two-step procedure. First, an internal surface of interest was exposed by cutting with an ultramicrotome (Tesla BS 490A). Next, that exposed surface was etched (1−2 h at room temperature) with a mixture containing 0.7 w/v of $KMnO_4$, dissolved in a 5:4:1 v/v mixture of 95% sulfuric acid, 85% phosphoric acid and distilled

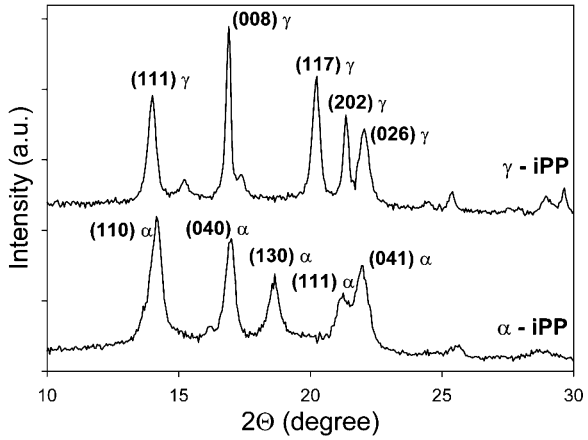

Figure 1. Diffractograms of α- and γ-crystalline modifications of iPP.

water, respectively, according to the procedure developed originally by Olley et al.[39] To improve etching, the mixture was placed in an ultrasonic bath running periodically for short time periods during the etching process. Etched, washed accordingly, and dried specimens[39] were coated with fine gold layer by ion-sputtering (JEOL JFC-1200) and examined with a scanning electron microscope (JEOL JSM-5500LV) operating in the high vacuum mode at accelerating voltage of 10 kV.

3. Results and Discussion

3.1. Phase Structure. Figure 1 presents diffraction curves of raw iPP, crystallized under atmospheric pressure and that of the same polymer crystallized isothermally at $T = 190$ °C and $p = 200$ MPa. Since most of the peaks characteristic for both α- and γ-phases are located at nearly the same positions[20] identification and calculation of the phase structure is difficult. The only difference between diffraction curves of α- and γ-crystals can be found in the range of $2\theta = 18-21°$, where two well-separated diffraction peaks of (130) plane of α-modification ($2\theta = 18.55°$) and (117) plane of γ-modification ($2\theta = 20.07°$) can be found. By comparison of the intensities of these peaks, the actual fraction of α- and γ-phases in the specimen can be estimated. Turner-Jones[9] proposed evaluation of the fraction of γ-modification in the crystalline component of the sample containing both α- and γ-crystals using the following equation

$$K_\gamma = \frac{I_\gamma(117)}{I_\gamma(117) + I_\alpha(130)} \quad (1)$$

where $I_\gamma(117)$ and $I_\alpha(130)$ denote integral intensities of the (117) and (130) diffraction peaks of γ- and α-modification, respectively. The parameter K_γ can vary within the range 0−1 for samples containing from 0 to 100% contribution of γ-modification. As can be inferred from Figure 1 iPP sample crystallized under atmospheric pressure does not contain any fraction of γ-form, while that crystallized at $T = 190$ °C and $p = 200$ MPa shows only γ-phase and no trace of α- or β-modifications (calculated phase parameter $K_\gamma = 0$ and 1, respectively). Similar analysis for other high-pressure samples, crystallized at lower temperature and/or pressure demonstrated mixed γ-/α-phase structure, with the phase parameter $K_\gamma = 0.82-0.98$.[40] Samples for further studies (morphology, deformation behavior) were prepared at conditions producing exclusively γ-phase ($K_\gamma = 1.0$), i.e., $T = 190$ °C and $p = 200$ MPa.

3.2. Morphology of γ-Phase. SEM observations of undeformed samples were performed to reveal their morphology. The representative micrographs obtained for iPP sample containing majority of γ-modification are presented in Figure 2, parts a and b. For comparison, the micrograph of the specimen of α-iPP, crystallized under atmospheric pressure at similar undercooling of 52 °C as γ-iPP, is also presented in Figure 2c (for γ-iPP, $T_m° = 242.1$ °C at 200 MPa;[25] hence, the undercooling at $T_c = 190$ °C is 52 °C). Microscopic observation demonstrated that in samples crystallized at high pressure the γ-lamellae are organized in spherulitic-like aggregates. These spherulites, although frequently immature, fill completely the sample volume. Lamellae within spherulites, packed in parallel stacks, spread radially and show only a moderate branching. The γ-spherulites do not show the "crosshatching" feature characteristic for α-spherulites grown under atmospheric pressure. Moreover, γ-spherulites, grown at high pressure are usually about 1 order of magnitude smaller than α-spherulites in the reference sample, which indicates reasonably higher rate of primary nucleation under elevated pressure ((cf. Figure 2, parts a and c; note that both samples were crystallized at the same undercooling of 52 °C resulting in quite similar crystallinities of 55 and 58.6 wt % for γ- and α-specimens, respectively).

SEM micrographs revealed also that the growth of γ-lamellae in a spherulite is most frequently initiated on some "seeds" of α-lamellae (cf. Figure 2b). Such a "seed" consists of a relatively long (up to a few micrometers) and thin parent lamella and several shorter branches growing out from this spine at angle of approximately 80°. Such branching, unique for the α-polymorph, develops by homoepitaxy on the (010) plane of a parent lamella, as schematically shown in Figure 2d. The (010) planes of both parent and daughter α-lamellae of such a "seed" constitute an ideal substrate for epitaxial growth of γ-lamellae—deposition of one layer rotated in-plane by 80°, which leads to near orthogonal branching in the α-phase, appears as the element of symmetry in the γ-form.[6,15,25] Lamellae of the γ-form branch at an angle of 40° to the surface of α-lamellae and the chains within γ-crystals are tilted at 40° to the lamellae normal (cf. Figure 2d). The orientation of γ-branching from the parent (spine) and transverse daughter lamellae is equivalent. Further growth of these γ-branches proceeds along the *c* axis, normal to the chain axis in γ-crystal, as well as to the plane of the α-seed. Such a type of epitaxial growth of γ-lamellae on those of the α-form was postulated to occur in crystallization of thin films[17] as well as bulk samples.[15,26]

Since neither X-ray phase analysis nor DSC revealed any trace of α-phase in samples studied it can be inferred that the growth of α-crystals is limited to the very initial phase of crystallization process and in the formation of seeds only. Further crystallization proceeds exclusively by epitaxial growth of γ crystals on these α-seeds. This leads soon to the formation of spherulitic aggregates filled completely with stacked γ-lamellae. Such a crystallization habit can suggest that the primary nucleation of the α-crystals must be significantly easier than for the γ-crystals, while further growth in the γ-form is favored under high-pressure conditions.

From the SAXS data, a long period of samples of γ- and α-iPP, both crystallized at the same undercooling of 52 °C, was determined: LP(γ) = 16.2 nm and LP(α) = 17.7 nm. From these and respective volumetric crystallinities, calculated from DSC data, the average thickness of lamellae, *l*, was estimated. The values of $l = 8.5$ and 9.9 nm were obtained for γ- and α-samples, respectively.

3.3. Stress—Strain Behavior. Figure 3 presents the true stress−true strain curves obtained for samples of γ-iPP ($X_c = 55$ wt %, LP = 16.2 nm and the estimated average lamellae thickness $l = 8.5$ nm) deformed in both plane-strain compression

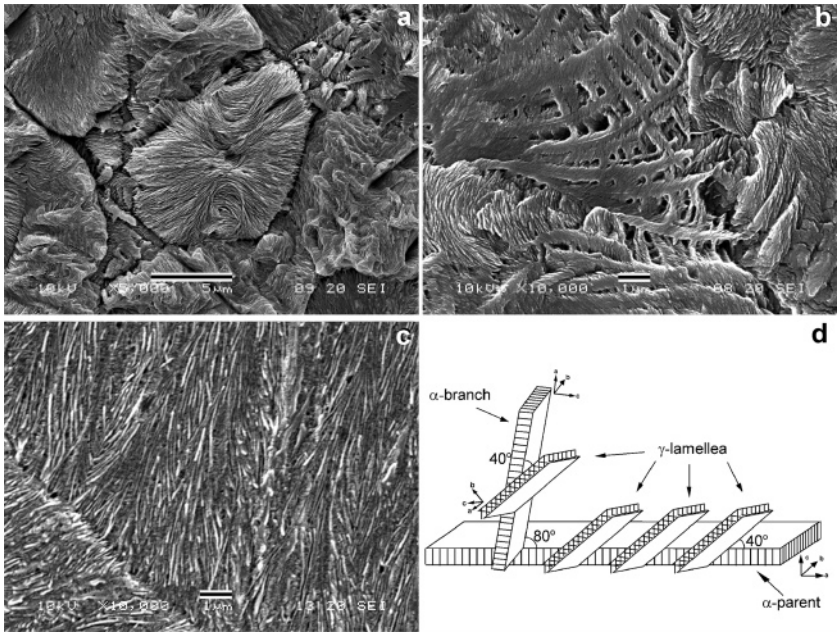

Figure 2. SEM micrographs of γ-iPP crystallized at high pressure (ab), α-iPP (c), and the schematic drawing illustrating the γ-branching from the α-"seed" (d) (modified from ref 15). Scale bars: 5 μm (a) and 1 μm (b, c).

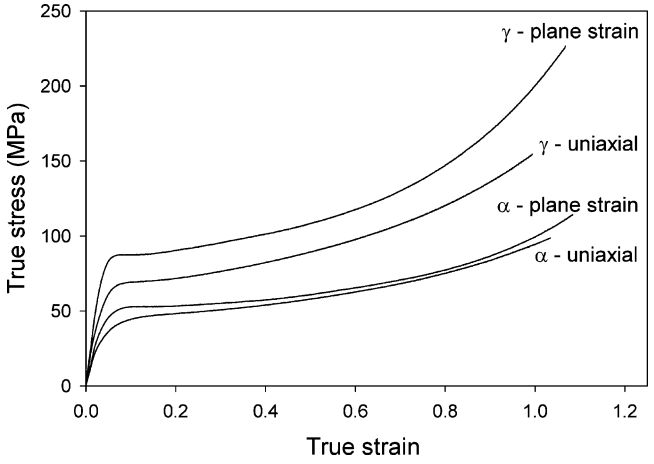

Figure 3. True stress−true strain curves determined for samples of α- and γ-iPP deformed in uniaxial and plane-strain compression with the constant true strain rate of 0.05 min^{-1} at room temperature.

Table 1. Mechanical Parameters Determined for Samples of α- and γ-iPP Deformed in Uniaxial and Plane-Strain Compression at Room Temperature

sample	Young modulus (GPa)	yield stress (by 2% offset) (MPa)	ultimate stress (MPa)	ultimate true strain
α-plane strain	1.28	49	113	1.09
α-uniaxial	1.13	37	96	1.02
γ-plane strain	2.25	86	214	1.02
γ-uniaxial	2.02	63	156	0.99

and uniaxial compression with constant strain rate of 0.05 min^{-1} at room temperature. For reference the curves of α-iPP (samples crystallized nonisothermally, exhibiting $X_c = 43$ wt %, LP = 12.6 nm, and $l = 5.2$ nm) deformed at identical conditions are presented. Mechanical properties evaluated from these compression tests are presented in Table 1.

The shape of all curves presented in Figure 3 is similar, typical for compression tests, with neither load nor true stress maximum near the yield and a distinct strain hardening stage. For a given crystal structure of samples, the stresses in plane-strain compression are higher than in uniaxial compression due to additional constraints present in plane-strain deformation mode. Moreover, there is an additional stress component arising from the friction between sample and the compression tool in the plane-strain compression test.

True stress−true strain curves of γ-iPP determined in both plane strain and uniaxial compression demonstrate significantly higher stress than respective curves of α-iPP in the entire strain range. The Young modulus determined for γ-samples is also higher than that of α. Higher modulus of γ-samples reflects most probably their higher crystallinity as compared to α samples: 55 vs 43 wt % for γ- and α-samples, respectively (as estimated from DSC data). The stress at yield is controlled primarily by the properties of the crystalline phase, including the lamella thickness.[41−45] Therefore, the higher yield and plastic flow stresses of γ-iPP can result from either larger thickness of γ-lamella ($l(\gamma) = 8.5$ nm while $l(\alpha) = 5.2$ nm) or from high plastic resistance (critical resolved shear stress) of γ-crystals, or from both. Crystals of γ-form are expected to have higher plastic resistance than α-crystals because of their specific structure with no parallel chain arrangement. This makes any crystallographic chain slip impossible. The only allowed crystallographic slip in this structure is the (001)[010] transverse slip, i.e., operating in the (001) plane, presumably exhibiting relatively high plastic resistance, since transverse slips show generally higher critical shear stresses than slips along the direction of chain[38] and because of an additional energy barrier arising from the specific structure of alternating bilayers in γ-crystals of iPP. In contrary, in α-modification crystallographic chain slips in (100) and (010) planes can operate quite easily.[46]

Another feature of the deformation behavior of γ-samples is the ultimate strain slightly lower than that observed in α-iPP. This will be discussed later in this section.

3.4. Evolution of the Structure upon Deformation. To follow the evolution of the structure and to find the operating deformation mechanisms several samples of γ-iPP deformed in plane-strain compression to the true strain of $e = 0.07$, 0.18, 0.41, 0.71, and 0.93 were prepared and examined.

Figure 4 presents SEM micrographs of the samples deformed to the indicated strain. The plane of the image is the LD−FD

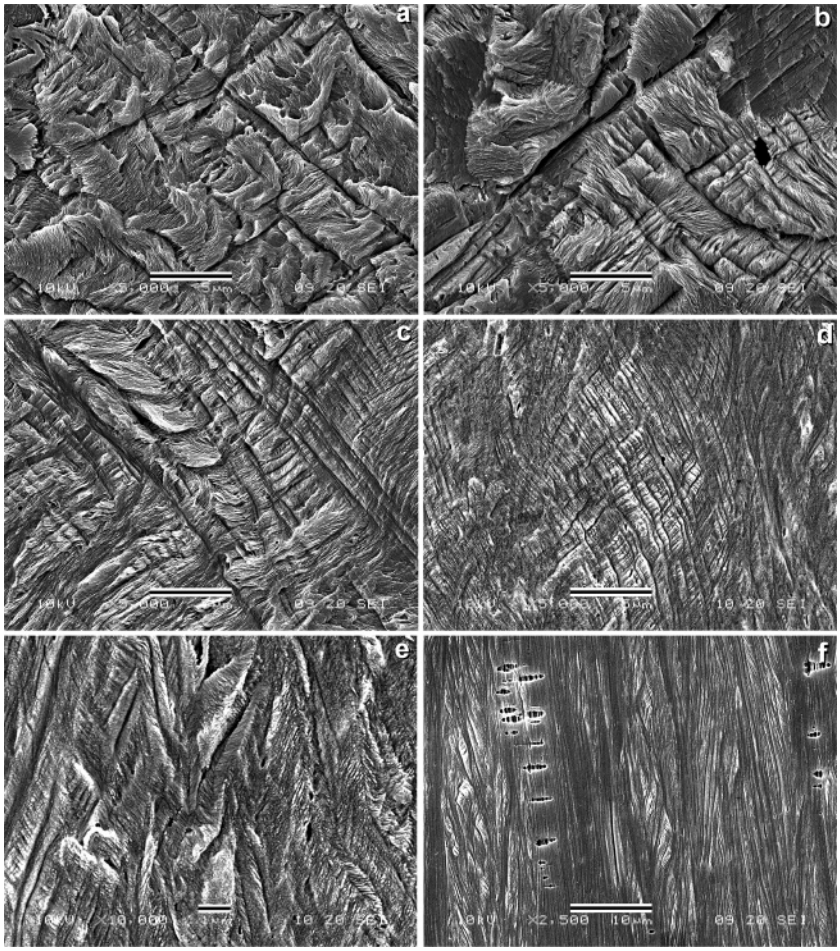

Figure 4. SEM micrographs of γ-iPP crystallized at high pressure and deformed in the plane-strain compression at room temperature to the true strain of 0.07 (a), 0.18 (b), 0.41 (c), 0.71 (d, e), and 0.93 (f). The plane of each micrograph is the LD-FD plane with the loading direction horizontal. Scale bars: 5 μm (a−d), 1 μm (e), and 10 μm (f).

plane, with the loading direction horizontal. The micrographs illustrate the formation of fine shear bands, appearing the primary deformation mechanism. The first bands can be observed on very early stages of plastic deformation (cf. Figure 4a, $e = 0.07$), probably created already at the yield. Bands are very long, crossing several adjacent spherulites and are inclined at the beginning of the deformation process approximately 45° with respect to the loading direction. With increasing strain the shear bands multiply and rotate gradually toward the flow direction. At high strains, $e = 0.7$ and higher, the dense collection of crossing shear bands fills completely the volume of the sample, destroying entirely the initial spherulitic morphology.

Examination of SEM micrographs indicates that shear bands are initiated by the shear within interlamellar amorphous layers. Propagating these bands across lamellae of other spherulites perpendicularly, destroys lamellae locally, which results in their fragmentation. At high strains ($e > 0.5$), the multiplication of shear bands followed by their rotation toward FD leads to quite heavy fragmentation of nearly all lamellae. The fragments between shear bands compressed along their long axes undergo kinking and rotation, which leads to a chevron-like morphology, illustrated in Figure 4e. This completes the transformation of the initial spherulitic morphology to the chevron-like arrangement of fragmented lamellae. Closer examination of micrographs revealed that the distances between lamellae, i.e., the thickness of the amorphous layers, frequently increase within those stacks of rotated lamellar fragments, which means that there must be a combination of the shear and tension along FD in the deformation of these amorphous layers.

Figure 4f shows the area of the sample deformed to $e = 0.93$ in the central flow region. Along with the structure of dense and heavily rotated shear bands one can observe here the initiation of a crazing-like fracture of the sample. The crazes, which develop only at high strains approaching $e = 1$, are oriented perpendicular to the direction of flow, i.e., to the direction of the highest extension. Nucleation and fast growth of crazes leads to relatively early fracture of γ-samples at true strain below $e = 1.0$ in both plane-strain and uniaxial compression, i.e., lower than α-samples deformed in similar conditions.

A DSC melting study of the deformed samples demonstrated that all samples exhibited a single melting peak with the maximum around 160 °C, which is characteristic for γ-modification. There was no trace of an α-peak or a high temperature shoulder on the main melting peak. However, in samples deformed to high strains of $e = 0.71$ and 0.93 a low endotherm around $T = 50$ °C can be recognized. It suggests a formation of the smectic phase[47] during plastic deformation. These features are illustrated in Figure 5a. Figure 5b shows the evolution of temperature of the melting peak and the crystallinity, determined from data of Figure 5a.

It can be seen that both the onset and the peak maximum temperatures practically do not depend on the strain applied, while the degree of crystallinity decreases from the initial 55 wt % to about 50 wt % at the true strain approaching 1.0. This shows that a reasonable part of the γ-crystals is destroyed during

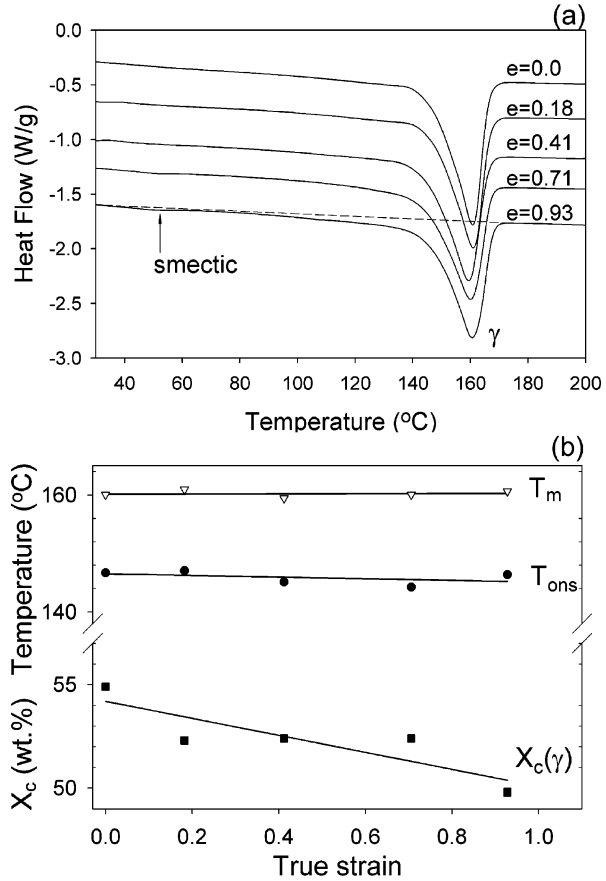

Figure 5. DSC thermograms of g-iPP samples deformed to true strain indicated (a) and the dependencies of temperature of the onset and maximum of the melting peak and overall crystallinity on the strain applied (b), determined from DSC data.

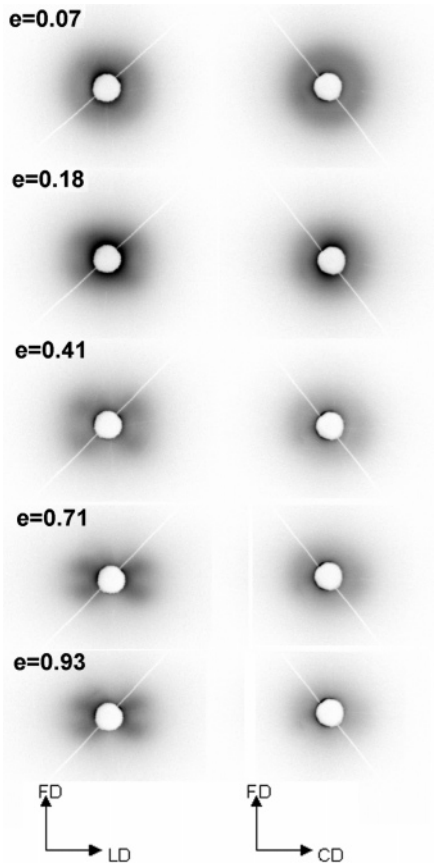

Figure 6. 2-D SAXS patterns of samples of γ-iPP deformed to the true strain indicated, recorded with X-ray primary beam parallel to CD (left) and to LD (right).

the plastic deformation, yet there is no formation of any new crystals of α-modification. Therefore, the stress-induced $\gamma-\alpha$ transformation, postulated long ago by Turner-Jones et al.[29] does not occur, at least in compression at room temperature. On the other hand, an occurrence of the smectic endotherm in deformed samples can suggest that a fraction of γ-crystals transforms to the mesophase upon deformation (confirmed by X-ray measurements, discussed later in this paper). It is probably associated with partial destruction of lamellae within fine shear bands reported above. It seems feasible that the destruction of crystalline order by advanced shear within bands leads to local transformation of crystalline phase into smectic.

The orientation of lamellae was probed with 2-D SAXS. Samples were illuminated by X-ray beam either from CD or LD direction. Recorded scattering patterns are presented in Figure 6. It can be seen that patterns observed in the CD-view evolve from a circular (undeformed sample, not shown), through elliptical ($e = 0.07$) to the 4-point pattern ($e = 0.18$ and above). At the same time patterns obtained in LD-view transform from circular to a weak and diffused 2-point pattern oriented along CD. While the intensity of scattering in CD-view patterns decreases slightly with increasing strain the intensity in LD-view patterns decreases much more rapidly. The appearance of 4-point signature in CD-view and fading away 2-point pattern observed in the LD-view can be attributed to the formation of preferred orientation of lamellae in two populations each oriented at some acute angle away from the direction of the flow, FD, typical for the chevron-like lamellar morphology. The angle between lamellar normals and FD estimated from the patterns of Figure 6 changes gradually with increasing strain from approximately 52° for $e = 0.18$, to nearly 70° for $e = 0.93$. The observed changes of scattering are consistent with microscopic observations of shear bands and formation of chevron-like lamellar morphology, reported earlier in this section.

The long period evaluated from LD-view 2-point patterns (estimation along CD, where maxima were found) remains practically constant in the entire strain range. In contrary, long period of deformed samples calculated from 4-point CD-view patterns, along directions set by the maxima, LP = 17−19 nm, is larger than LP = 16.2 nm, found in the initial undeformed material. That increase is connected apparently with an increase of the distance between fragmented lamellae confined by adjacent shear bands, occurring on their kinking and rotation producing a chevron morphology, which was observed microscopically (cf. Figure 4e)

DSC data reported above suggested an appearance of the smectic phase in the deformed samples. To check that and to estimate the amount of smectic phase formed, the phase composition of samples deformed to various strains was evaluated from X-ray diffraction data. Because of crystal texture developing in deformed samples the phase analysis had to include collection of diffraction data for various orientation of the sample with respect to the primary beam, to take into account contributions of different populations of oriented crystallites. For a raw estimation of the phase structure we decided to measure samples in 12 orientations each, preselected on the basis of texture analysis (reported later in this section). That selection was a compromise between accuracy of the estimation and the time needed for measurements and calculations. Every specimen tested was positioned in the diffractometer cradle at a polar angle

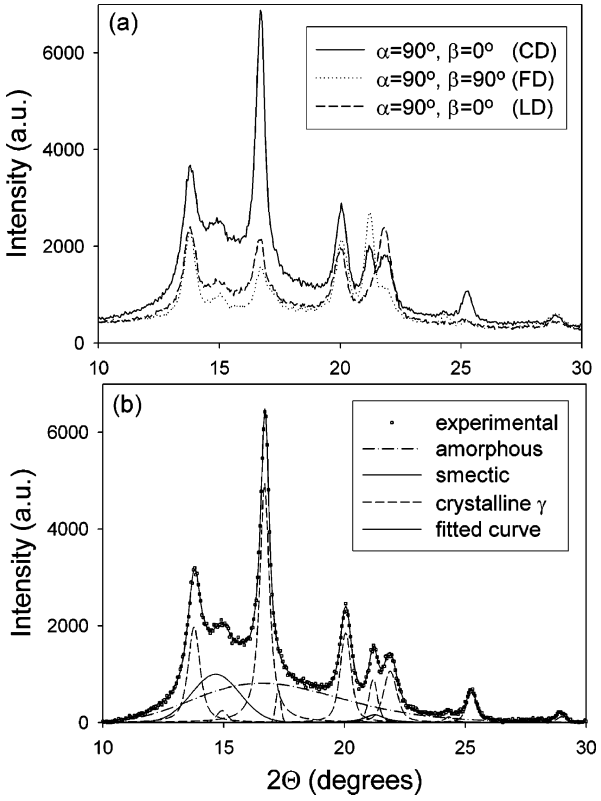

Figure 7. Diffractograms of the sample of γ-iPP deformed to the strain $e = 0.93$, recorded for various angular position of the specimen in the diffractometer, as indicated (a) and an example of the peak separation applied to experimental data (b).

of $\alpha = 0$, 30, 60, or 90° and an azimuth angle of $\beta = 0$, 45, or 90°. For each position (orientation) of the specimen the diffraction curve was measured. Next, the contributions of crystalline γ and α, the smectic and amorphous components, respectively, were calculated from every diffractogram using the peak separation procedure. Finally, spatially average values of every phase contribution to the composition phase composition were calculated from these data for all samples.

Figure 7a illustrates the variation of the diffraction curve with the orientation of the sample with respect to the primary beam. In addition to the variation of the intensity of crystalline peaks one can observe here quite a large variation of the intensity around $2\theta = 15°$ related primarily to the presence of oriented smectic phase and an amorphous component. Figure 7b shows an exemplary result of the peak separation applied to the experimental data. From the calculated area of relevant peaks the phase composition was estimated in the way described above.

The results of the estimation of the phase composition, averaged over orientation space, are shown in Figure 8. The estimates show that the crystalline phase consist entirely of crystals of γ-modification, with no trace of α-modification regardless of the strain applied. The amount of the γ-phase, represented by the degree of crystallinity, X_c, stays initially constant and decreases above $e = 0.2-0.3$. The decreasing trend is similar to that observed in crystallinity estimated from the DSC data (Figure 5), although the values obtained from X-ray analysis are generally higher than those from DSC. Note that similar discrepancy has been frequently reported for iPP: to get an agreement between X-ray and DSC based crystallinity one should use the value of the heat of melting of crystalline phase $\Delta H_f = 167$ J/g rather than the widely accepted value of 209 J/g for α-phase or 144.8 J/g instead of 190 J/g for the γ-modification.[25] This was also the case here: when using ΔH_f

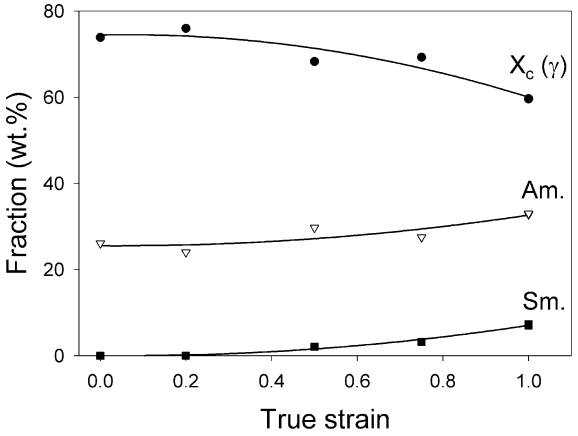

Figure 8. Dependence of average contributions of crystalline (γ), smectic, and amorphous phases on the strain applied, determined from diffraction data using peak separation procedures.

$= 144.8$ J/g[25] for calculations an agreement between X-ray and DSC based estimations was noticed.

Along with decreasing crystallinity a slight increase of the amorphous fraction and formation of a new smectic component is observed at the true strain above $e = 0.2$. This mesophase is observed first in the sample deformed to the true strain of $e = 0.41$ (smectic fraction, $\phi_{sm} = 2\%$). In highly deformed sample of $e = 0.93$ the amount of smectic modification increases, giving the spatially averaged value of smectic content of $\phi_{sm} = 7.2\%$. At the same time, an estimated amount of the amorphous phase is about 6.7% higher than that found in the initial undeformed material. This means that a little more than a half of the destroyed crystals are transformed into the smectic component, with only partially destroyed ordering, while the remaining part is transformed into less ordered amorphous material. Interestingly, the highest content of the mesophase, estimated for this sample in the direction of CD is above 19%, while very little smectic phase is detected in LD or FD. On this basis, the preferred orientation of the smectic phase with the layer normal close to CD can be anticipated.

Development of the crystalline texture in the deformed samples was monitored with pole figures. Figure 9 presents the set of pole figures constructed for the crystallographic planes of (111), (008), and (117) of the orthorhombic γ-iPP in samples deformed to the true strain of 0.18, 0.41, 0.71, and 0.93, respectively.

It can be observed that the γ crystalline component develops a texture with the increase of strain. This texture is relatively weak—at the true strain of $e = 0.93$ the highest intensity (concentration of poles in the CD direction in (008) pole figure) slightly exceeds the doubled intensity of the random distribution. Pole figures of samples deformed to $e = 0.18$, 0.41, and 0.71 illustrate a gradual development of the final texture, seen in the sample of $e = 0.93$. This final texture is consistent with a weak one-element texture of the dominating crystal orientation with the *c* axis oriented along CD, *b* axis oriented approximately 10−30° away from LD toward FD and *a* axis ca. 10−30° away from FD. Such orientation is expected to give the maxima along CD in the (008), approximately 60−80° away from LD toward FD in the (111) and between CD and FD in the (117) pole figures, respectively, which are in fact observed experimentally (cf. Figure 9). In addition to those, one can notice in the experimental pole figures, especially those for low strains, some additional maxima located around the polar region (LD), but these can be assigned to artifacts, produced most probably by the sample geometry.

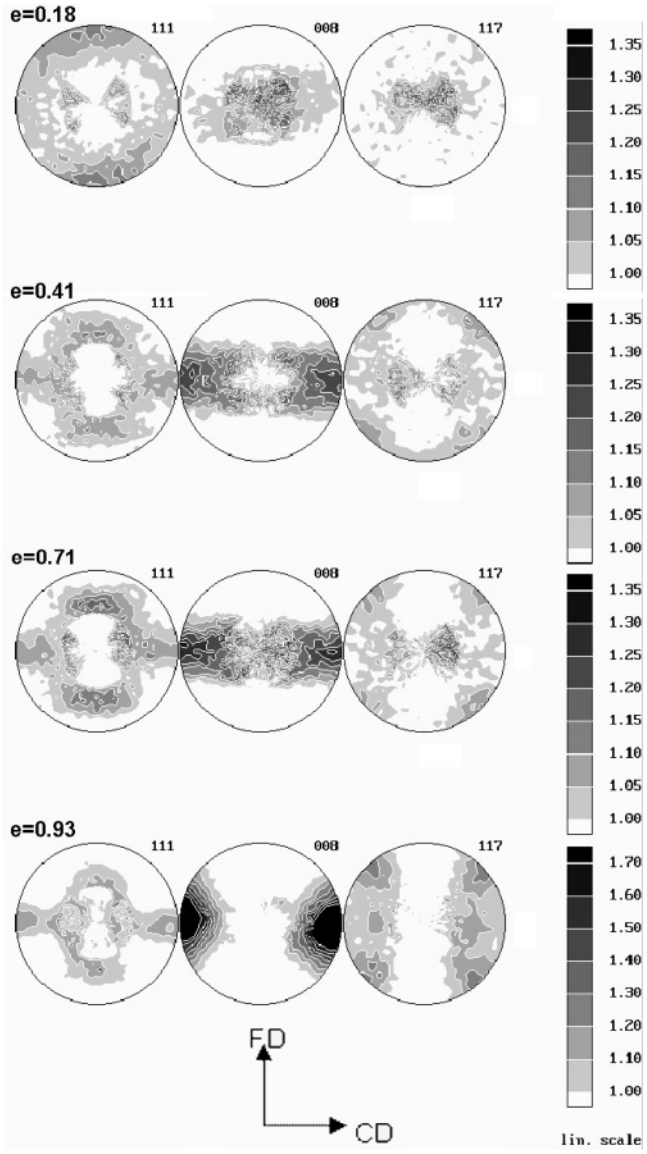

Figure 9. Pole figures of (111), (008), and (117) planes of orthorhombic y-iPP determined for samples deformed in plane-strain compression to true strain indicated.

The postulated texture develops by gradual rotation of crystallites around the *c* axis—at the strain of $e = 0.18$ the expected direction of *b* axis makes an angle with LD roughly 40° and then rotates toward LD to the position about 20° away from LD when the true strain reaches 0.93 (both positions derived from experimental pole figures). Since the *b* axis coincides with the lamellar normal in γ-crystals it can be concluded that the rotation of crystallites deduced from pole figures agrees very well with that found in the analysis of SAXS patterns, presented in Figure 6: the angle between lamellar normal and LD changed from 37 to 22° with the strain advance from 0.18 to 0.93. That result demonstrates also that the main deformation mechanism giving rise to the development of both crystal texture and lamellar orientation was the interlamellar shear proceeding in the amorphous interlamellar layers. There is practically no evidence of activity of any crystallographic deformation mechanism within crystalline component, including the (001)[010] transverse slip, which was considered earlier as the probable mechanism for this crystal structure. It means that the plastic resistance of that anticipated slip system is too high to be activated during deformation by compression.

The crystalline texture of γ samples developed in the plane-strain compression is much weaker than the sharp two-component texture ((010)[001] and (110)[001]), observed in compressed samples of α-iPP [46] or quasi-single-crystal texture (100)[001] observed in polyethylene.[30] The sharp textures in α−iPP or PE are, however produced primarily by several highly active crystallographic slip mechanisms along the direction of chain,[30,46] which mechanisms are prohibited in γ−crystals due to their unique structure.

4. Conclusions

The experimental work reported in this communication allowed to obtain bulk samples of iPP homopolymer in which the major crystalline phase was the γ-modification. Crystallization under the pressure of 200 MPa and temperature of 190 °C allowed to obtain samples containing exclusively γ-crystal modification with only a minor trace of α-crystals.

It was found that the growth of γ-lamellae is most frequently initiated on some "seeds" consisting of a spine of single α-lamella and several shorter α-lamellae branching at the angle of 80° from that spine. On such an α-"seed", many shorter γ-lamellae start to grow normally, through epitaxy on (010) faces of α-parent and daughter lamellae. Further growth of these γ-lamellae with only minor noncrystallographic branching leads to the formation of immature spherulites, which fill completely the volume of the sample.

Plastic deformation experiments on samples containing exclusively γ-form crystals, performed in the plane-strain compression, demonstrated higher elastic modulus, yield stress, and flow stress yet slightly lower ultimate strain than the samples containing crystals of α modification.

During plastic deformation numerous fine shear bands, initiated by the interlamellar shear of the amorphous layers are formed in the compressed sample. These bands most probably are initiated already at the yield point. Propagation of the bands across the sample causes the local destruction of the encountered lamellae which were not oriented parallel to the direction of the developing band. The destroyed fragments of crystallites transform partially into the smectic phase. This leads eventually to the reduction of the overall crystallinity by approximately 14 wt % (at the true strain of $e = 0.93$), from which more than a half is transformed into mesophase. No γ−α phase transformation was detected.

With increasing strain the shear bands multiply considerably and tilt toward the flow direction. The lamellae already fragmented by the local destruction occurring within shear bands undergo kinking followed by rotation due to interlamellar shear (lamella normal equivalent to the crystallographic *b* axis rotates toward the load direction), resulting in the formation of a chevron-like lamellar arrangement. This leads to the development of a 4-point signature in SAXS patterns of the samples deformed above $e = 0.2$. At the same time the relatively weak one-component crystalline texture is developed. The main component of this texture is described by the orientation of *c* crystallographic axis along CD, *b* axis approximately 10−30° away from LD toward FD and *a* axis 10−30° away from FD. Both crystalline texture and lamellae orientation develop due to the activity of the same deformation mechanism, identified as the interlamellar slip produced by the shear within interlamellar amorphous layers. That shear is relatively easy since lamella are arranged in parallel stacks, with neither "crosshatching" characteristic for the α-structure nor any serious noncrystallographic branching, which could be potential obstacles for that slip. Any crystallographic deformation mechanism within

crystalline component, including the (001)[010] transverse slip, the only slip anticipated for γ-crystals, were not detected in deformation experiments performed within this study, which suggests the relatively high plastic resistance of that crystallographic slip mechanism.

It is concluded that the interlamellar shear of the amorphous layers appears the easiest and therefore becomes the primary deformation mechanism of γ-iPP. Numerous shear bands are initiated by that interlamellar slip. The other identified mechanism, the γ-to-smectic phase transformation, associated with shear banding, plays rather a minor, supplementary role in the deformation sequence.

Acknowledgment. This work was financed in part from the budget sources for science in the years 2005−2008 as a research project (Grants 3 T08E007 28 and 3 T08E008 30).

References and Notes

(1) Natta, G.; Corradini, P. *Nuovo Cimento Suppl.* **1960**, *15*, 40−51.
(2) Karger-Kocsis, J, Ed. *Polypropylene Structure, blends and composites*; Chapman & Hall: London, 1995.
(3) Padden, F. J.; Keith, H. D. *J. Appl. Phys.* **1966**, *37*, 4013−4020.
(4) Norton, D. R.; Keller, A. *Polymer* **1985**, *26*, 704−716.
(5) Addink, E. J.; Beintema, J. *Polymer* **1961**, *2*, 185−193.
(6) Lotz, B.; Graff, S.; Wittmann, J. C. *J. Polym. Sci., Part B: Polym. Phys. Ed.* **1986**, *24*, 2017−2032.
(7) Morrow, D. R.; Newman, B. A. *J. Appl. Polym. Sci.* **1968**, *39*, 4944−4950.
(8) Kojima, M. J. *J. Polym. Sci. Part B: Polymer Lett.* **1967**, *5*, 245−250.
(9) Turner-Jones, A. *Polymer* **1971**, *12*, 487−507.
(10) Guidetti, G. P.; Busi, P.; Giulianetti, I.; Zanetti, R. *Eur. Polym. J.* **1983**, *19*, 757−759.
(11) Busico, V.; Corradini, P.; De Rosa, C.; Di Benedetto, E. *Eur. Polym. J.* **1985**, 2*1*, 239−244.
(12) Avella, M.; Martuscelli, E.; Della Volpe, G.; Segre, A.; Rossi, E.; Simonazzi, T. *Makromol Chem.* **1986**, *187*, 1927−1943.
(13) Marigo, A.; Marega, C.; Zanetti, R.; Paganetto, E.; Canossa, E.; Coleta, F.; Gottardi, F. *Makromol Chem.* **1989**, *190*, 2805−2813.
(14) Mezghani, K.; Phillips, P. J. *Polymer* **1995**, *35*, 2407−2411.
(15) Hosier, I. L.; Alamo, R. G.; Lin, J. S. *Polymer* **2004**, *45*, 3441−3455.
(16) Fischer, D.; Mülhaupt, R. *Makromol. Chem. Phys.* **1994**, *195*, 1433−1441.
(17) Thomann, R.; Wang, Ch.; Kressler, J.; Mülhaupt, R. *Macromolecules* **1996**, *29*, 8425−8434.
(18) Meille, S. V.; Ferro, D. R.; Brückner, S.; Lovinger, A. J.; Padden, F. J. *Macromolecules* **1994**, *27*, 2615−2622.
(19) Brückner, S.; Meille, S. V. *Nature (London)* **1989**, *340*, 455−457.
(20) Meille, S. V.; Brückner, S.; Porzio, W. *Macromolecules* **1990**, *23*, 4114−4121.
(21) Brückner, S.; Meille, S. V.; Sozzani, P.; Torri, G. *Macromol. Chem. Rapid Commun.* **1990**, *11*, 55−60.
(22) Brückner, S.; Philips, P. J.; Mezghani, K.; Meille, S. V. *Macromol. Rapid Commun.* **1997**, *18*, 1−7.
(23) Ferro, D. R.; Brückner, S.; Meille, S. V.; Ragazzi, M. *Macromolecules* **1992**, *25*, 5231−5235.
(24) Campbell, R. A.; Phillips, P. J.; Lin, J. S. *Polymer* **1993**, *34*, 4809−4916.
(25) Mezghani, K.; Phillips, P. J. *Polymer* **1998**, *39*, 3735−3744.
(26) Mezghani, K.; Phillips, P. J. *Polymer* **1997**, *38*, 5725−5733.
(27) Lotz, B.; Graff, S.; Straupé, C.; Wittmann, J. C. *Polymer* **1991**, *32*, 2902−2910.
(28) Turner, J. D.; Lingafelter, E. C. *Acta Crystallogr.* **1955**, *8*, 551−557.
(29) Turner-Jones, A.; Aizlewood, J. M.; Beckett, D. R. *Macromol. Chem.* **1964**, *75*, 134−158.
(30) Galeski, A.; Bartczak, Z.; Argon, A. S.; Cohen, R. E. *Macromolecules* **1992**, *25*, 5705−5718.
(31) Psarski, M.; Piorkowska, E.; Galeski, A. *Macromolecules* **2000**, *33*, 916−932.
(32) Young, R. J.; Bowden, P. B.; Ritchie, J. M.; Rider, J. G. *J. Mater. Sci.* **1973**, *8*, 23−36.
(33) Bartczak, Z.; Kozanecki, M. *Polymer* **2005**, *46*, 8210−8221.
(34) Brandrup, J., Immergut, E. H., Grulke, E. A., Eds. *Polymer Handbook*, 4th ed.; Wiley-Interscience: New York, 1999.
(35) Rabiej, M. *Polimery* **2002**, *47*, 423−427.
(36) Rabiej, M. *Polimery* **2003**, *48*, 288−295.
(37) Alexander, L. E. *X-ray Diffraction Methods in Polymer Science*; Wiley-Interscience: New York, 1969.
(38) Bartczak, Z.; Argon, A. S.; Cohen, R. E. *Macromolecules* **1992**, *25*, 5036−5053.
(39) Olley, R. H.; Hodge, A. M.; Bassett, D. C. *J. Polym. Sci., Polym. Phys. Ed.* **1979**, *17*, 627−643.
(40) Lezak, E.; Bartczak, Z. *Fibres Text. E. Eur.* **2005**, *13*, 51−56.
(41) Young, R. J. *Mater. Forum* **1988**, *11*, 210−218.
(42) Crist, B. *Polym. Commun.* **1989**, *30*, 69−71.
(43) Brooks, N. W. J.; Mukhtar, M. *Polymer* **2000**, *41*, 1475−1480.
(44) Kazmierczak, T.; Galeski, A.; Argon, A. S. *Polymer* **2005**, *46*, 8926−8936.
(45) Argon, A. S.; Galeski, A.; Kazmierczak, T. *Polymer* **2005**, *46*, 11798−11805.
(46) Pluta, M.; Bartczak, Z.; Galeski, A. *Polymer* **2000**, *41*, 2271−2288.
(47) Wang, Z. G.; Hsiao, B. S.; Srinivas, S.; Brown, G. M.; Tsou, A. H.; Cheng, S. Z. D.; Stein, R. S. *Polymer* **2001**, *42*, 7561−7566.

MA0605907